Modeling the phase behavior of polydisperse rigid rods with attractive interactions, with applications to SWNTs in super acids

Micah J. Green<sup>1</sup>, A. Nicholas G. Parra-Vasquez<sup>1</sup>,

Natnael Behabtu<sup>1</sup>, Matteo Pasquali<sup>1,2\*</sup>

<sup>1</sup>Dept. of Chemical and Biomolecular Engineering, <sup>2</sup>Dept. of Chemistry

Rice University

6100 Main Street, MS362

Houston TX 77005

\*mp@rice.edu

December 17, 2021

#### Abstract

The phase behavior of rodlike molecules with polydisperse length and solventmediated attraction and repulsion is described by an extension of the Onsager theory for rigid rods. A phenomenological square-well potential is used to model these long-range interactions, and the model is used to compute phase separation and length fractionation as a function of well depth and rod concentration. The model closely captures experimental data points for isotropic/liquid crystalline phase coexistence of single-walled carbon nanotubes (SWNTs) in superacids. The model also predicts that the isotropic-biphasic boundary approaches zero as acid strength diminishes, with the possibility of coexistence of isotropic and liquid crystalline phases at very low concentrations; this counterintuitive prediction is confirmed experimentally. Experimental deviations from classical theories for rodlike liquid crystals are explained in terms of polydispersity and the balance between short range repulsion and long range attractions. The predictions of the model also hold practical import for applications of SWNT/superacid solutions, particularly in the processing of fibers and films from liquid crystalline SWNT/superacid mixtures.

# 1 Introduction

When suspended in a liquid, rodlike molecules and particles transition from an isotropic, disordered state to an aligned, liquid-crystalline nematic state at sufficiently high concentration. This classical, peculiar behavior has generated numerous theories for predicting the isotropic-nematic transition and the equilibrium properties of the coexisting phases; typically, these theories treat the rodlike molecule or particle as an idealized Brownian rigid rod of high aspect ratio. These theories capture with some success the behavior of classical lyotropic liquid-crystalline materials such as liquid crystalline polymer solutions and rodlike biological particles in water [1]. However, previous theoretical studies fail to describe dispersions of novel anisotropic nanomaterials such as single-walled carbon nanotubes (SWNTs). Here we extend the theoretical description of polydisperse Brownian rods to include the competition

of short-range repulsion and long-range attraction that is known to yield rich behavior in colloidal phases. We focus on the coexistence between the isotropic and nematic phases.

### 1.1 Isotropic-Nematic Phase Separation

In 1949, Onsager developed a statistical mechanical theory for the rod orientation distribution function in order to describe the phase behavior of idealized monodisperse rods interacting via a mean field excluded-volume potential in an athermal solvent [2]. This theory is based on the competition between the orientational entropic contribution to the free energy and the excluded-volume potential. This competition gives rise to the isotropic-nematic phase transition that is characteristic of many rodlike molecules. As rods crowd beyond a critical concentration, alignment occurs spontaneously because orientational ordering is accompanied by a loss of interaction free energy which offsets the partial gain of free energy due to loss in orientational entropy. The predicted coexistence of an isotropic phase and an aligned phase is observed in experimental systems. Onsager's original formulation was numerically refined by Kayser and Raveché [3] and Lekkerkerker et al [4]. Later studies extended Onsager's approach to nonhomogeneous systems in order to resolve the profile of the interface between bulk isotropic and nematic regions [5, 6, 7] and finite-sized regions Onsager's approach was also modified to include attractive interactions via a simple order-parameter-based attractive potential by Khokhlov and Semenov [9, 10].

The major competing theoretical framework for rigid rod phase behavior is Flory's latticebased theory [11], which accounts for excluded-volume interactions via packing effects and allows for attractive inter-particle interactions governed by the parameter  $\chi$ . Flory's predictions for the boundaries of the well-known biphasic chimney for an athermal solvent ( $\chi = 0$ ) are slightly higher (7.89d/L, 11.57d/L) than the Onsager predictions (3.29d/L, 4.19d/L), where d and L are the rod diameter and length, respectively. As the attractive force increases, the biphasic region broadens and the concentration of the coexisting aligned phase grows dramatically such that the coexistence nematic phase is a solid. (The results of Khokhlov [9] show a similar broadening effect.) The lattice-based Flory theory allows for great versatility in describing a variety of systems, including mixtures and various types of molecules. Flory and others used the lattice framework to extend models to semiflexible rods [12], mixtures of rods and flexible coils [13], rods connected by flexible linkers [14], rods with flexible side chains [15], and, most relevant to the present study, polydisperse rods [16].However, the myriad numerical approximations inherent in Flory's treatment have limited the quantitative applications of the theory to anisotropic nanoparticles [17], particularly those that interact differently at long and short ranges. Moreover, the "attractive" interactions in Flory's theory simply indicate the enthalpy of mixing. In a poor solvent, the rods tend to "attract" one another simply because of the poor compatibility between rod and solvent. This attraction only acts on molecules immediately bordering the rod in the lattice, i.e., at short ranges.

Other efforts to describe attractive interactions between rods typically focus on depletion forces caused by non-adsorbing polymers in solution with the rods. Surve *et al.* modeled the effects of adsorption in a Flory-like framework [18], while Bolhuis *et al.* used particle-based simulations to simulate spherocylinders with depletion forces caused by the addition of nonadsorbing polymer [19].

### 1.2 Effects of Polydispersity

In a system of rods, length polydispersity broadens the biphasic region, and long rods preferentially enter the nematic phase, as intuited by Onsager. Moreover, the coexisting isotropic and nematic concentrations depend strongly on the initial (or "parent") concentration of rods. In a solution of monodisperse rods, these coexistence concentrations are independent of the parent concentration; in a solution of polydisperse rods, the increased degree of freedom in the length-dimension yields much richer phase behavior.

Speranza and Sollich computed the coexistence concentrations of a system of Onsager rods with continuous polydispersity in length [20], but the most thorough and accurate analysis of this problem is the 2003 study by Wensink and Vroege [21]. Wensink and Vroege numerically computed the biphasic boundaries as a function of the initial concentration and the degree of polydispersity. Notably, they found that, as polydispersity increases, the isotropic boundary moves to lower concentrations, and the nematic boundary shifts to dramatically higher ones, broadening the biphasic region. They also identified specific scenarios where a triphasic (isotropic, short rod nematic, long rod nematic) equilibrium state can occur. Although the numerical analysis in [21] was limited to two forms of the parent population with varying polydispersity, the theory applies to systems described by any rod length distribution.

These studies of polydisperse rod systems were limited to athermal solvents; here we aim to extend this work to include the effect of long-range attraction combined with short-range repulsion.

### 1.3 Experimental Motivation

The present study is motivated by recent experimental results on the phase behavior of single-walled nanotubes (SWNTs) dispersed in superacids, such as fuming sulfuric acid and chlorosulfonic acid [22, 23, 24, 17]. Since Iijima et al's observation of SWNTs in 1993 [25], SWNTs have attracted great interest because of their unique electronic and mechanical properties [26]; much current research is devoted to the creation of neat SWNT macroscopic articles with properties comparable to the constituent SWNTs. However, the production of such macroscopic articles has been hindered by the difficulty of dispersing SWNTs as individual rods.

The dispersion of SWNTs is difficult because they tend to bundle tightly due to strong van der Waals attraction to each other. Few solvents disperse pristine SWNTs as individual rods capable of forming a concentrated liquid-crystalline phase. SWNTs can form a liquid crystalline solution in water when wrapped or stabilized by acids containing hydrophobic groups such as DNA or hyaluronic acid [27, 28] or when trapped in hydrogels [29]. Superacids, such as fuming sulfuric acid and chlorosulfonic acid, are the only fluids that spontaneously disperse SWNTs as individual rods in a concentrated liquid crystalline state [22, 24, 17]. Superacids protonate the sidewalls of SWNTs and cause electrostatic repulsion and debundling [23]. These liquid crystalline dopes have been used for the production of macroscopic SWNT articles [30, 17, 31].

Surprisingly, in superacids weaker than (roughly) equimolar mixtures of sulfuric and chlorosulfonic acids, liquid-crystalline domains are in equilibrium with a dilute isotropic phase. These liquid-crystalline domains are endless, threadlike structures, termed "SWNT"

spaghetti," composed by a myriad of aligned SWNTs spaced by a few SWNT diameters. The SWNTs can translate along the axis of the strand, but have very limited mobility in the normal direction. This unusual phase behavior cannot be described by the Onsager or Flory theories for monodisperse rods because the SWNTs are polydisperse and because the theories cannot accurately describe the effects of varying acid strength on the inter-rod interactions. In fact, the broadening of the biphasic chimney occurs on the isotropic side rather than the nematic side, contrary to Flory's predictions.

Modeling the phase behavior of such systems would involve both electrostatic forces due to protonation and inter-SWNT van der Waals attraction. The balance of electrostatic repulsive interactions and van der Waals attractive interactions for dilute polyelectrolyte colloids have been modeled using the Derjaguin, Landau, Verwey, and Overbeek (DLVO) theory [32, 33]. The DLVO approach was generalized for interactions between charged anisotropic macromolecules by Chapot et al [34]. The DLVO approach has been applied to a number of experiments on aqueous suspensions of charged rods such as V<sub>2</sub>O<sub>5</sub> gels [35] and b-FeOOH [36]. DLVO and similar theories cannot be applied to rods in superacids because the assumption of dilute electrolytes inherent in the DLVO theory are inapplicable.

We postulate that the key physical mechanism controlling the behavior of SWNTs in acids is the competition between long-range van der Waals attraction, which is weakly dependent on acid strength, and short-range electrostatic repulsion, which depends strongly on acid strength—as shown clearly by Raman spectroscopy of SWNTs in acids. We approximate this competition through a simple inter-rod repulsive-attractive potential, where strength of the attractive well varies with solvent quality. The rods interact through an attractive force that varies inversely with acid strength; this attractive force mimics van der Waals

interactions offset to varying degrees by electrostatic repulsion as a function of protonation.

# 2 Formulation

### 2.1 Free Energy

Our formulation follows that of Wensink and Vroege and includes an additional potential to capture the effect of attractive interparticle interactions and solvent effects. A solution of thin rigid rodlike molecules of diameter d and polydisperse lengths L is described by a rod distribution function N(l). N(l) refers to the number of rods in the system with relative length l, where l is defined as  $L/L_0$  and  $L_0$  is an arbitrary reference length. For a volume V, N(l)/V is the local number density of rods of length l, and  $\int N(l)dl$  gives the total number of rods in the system.

The dimensionless Onsager excess free energy f for a volume V is written as

$$f = \frac{bF}{Vk_BT} \sim \int c(l)[\ln c(l) - 1]dl + \int c(l)\omega(l)dl$$
$$+ \int \int c(l)c(l')ll'[\rho(l,l') + \lambda(l,l')]dldl', \tag{1}$$

where the reference volume b is defined as  $\pi dL_0^2/4$ , and the dimensionless rod distribution function c(l) is defined as bN(l)/V. The total rod number concentration is  $c_0$ , the zeroth moment of the distribution c(l), where distribution moments are defined as

$$c_k = \int c(l)l^k dl. (2)$$

The overall concentration of the system can also be described by the rod volume fraction  $\phi = (d/L_0)c_1$ . The rod volume fraction is a more experimentally accessible quantity.

The entropic terms in the free energy description can be described as follows. The first term describes the ideal free energy of the polydisperse system. The second term contains the orientational entropy contribution,

$$\omega(l) = \int \psi(l, \mathbf{u}) \ln[4\pi\psi(l, \mathbf{u})] d\mathbf{u}, \tag{3}$$

where  $\psi(l, \mathbf{u})$  is the normalized angular distribution function for rods with relative length l with orientation described by the unit vector  $\mathbf{u}$ . This term is minimized by a uniform (isotropic) distribution of rod angles written as  $\psi = 1/4\pi$ . The third term contains the excluded volume interactions between rods. The average excluded volume contribution from rods of relative length l and l' is

$$\rho(l, l') = \int |\mathbf{u} \times \mathbf{u}'| \psi(l, \mathbf{u}) \psi(l', \mathbf{u}') ] d\mathbf{u}' d\mathbf{u}. \tag{4}$$

This term equals 1 for an isotropic state and is minimized by an aligned nematic state where the rods' alignment minimizes their excluded-volume interactions. The attractive/repulsive potential  $\lambda(l, l')$  models inter-rod attraction and repulsion, and is new. The phase behavior of idealized Onsager rods is governed by the balance between  $\omega(l)$  and  $\rho(l, l')$  as a function of c(l).

We follow Wensink and Vroege in using the uniaxial Gaussian ansatz to approximate the angular distribution function  $\psi(l, \mathbf{u})$ , written as

$$\psi(l, \mathbf{u}) = \begin{cases} \frac{\alpha(l)}{4\pi} \exp\left[-\frac{1}{2}\alpha(l)\theta^2\right] & \text{for } 0 \le \theta \le \pi/2\\ \frac{\alpha(l)}{4\pi} \exp\left[-\frac{1}{2}\alpha(l)(\pi - \theta)^2\right] & \text{for } \pi/2 \le \theta \le \pi \end{cases}$$
(5)

such that  $\psi(l, \mathbf{u})$  is reduced to an unknown in only the l-dimension through the function  $\alpha(l)$ . The function  $\alpha(l)$  is left as an unknown that describes the degree of alignment in a

given phase. Because of their higher excluded-volume cost, longer rods tend to be more aligned. Wensink and Vroege develop an asymptotic expansion of  $\rho(l, l')$  for the nematic phase in terms of  $\alpha$  as

$$\rho(l, l') \sim \sqrt{\frac{8}{\pi} \left(\alpha(l)^{-1} + \alpha(l')^{-1}\right)},$$
(6)

where terms involving higher powers of  $\alpha(l)^{-1}$  are neglected.

We designate variables as pertaining to the isotropic phase, nematic phase, and parent phase by using the superscripts (I), (N), and (0) for the theoretical description of a parent population  $c^{(0)}(l)$  phase separating into  $c^{(I)}(l)$  and  $c^{(N)}(l)$ .

### 2.2 Equilibrium Conditions

The degree of alignment for any nematic equilibrium state must minimize the free energy. In the present case, the degree of alignment is expressed through the unknown  $\alpha(l)$ , and the condition is written as

$$\frac{\delta f}{\delta \alpha(l)} = 0 = \frac{c(l)}{\alpha(l)} - \left(\frac{8}{\pi}\right)^{1/2} \frac{lc(l)}{2\alpha^2(l)} \int l'c(l')dl + lc(l) \int l'c(l') \frac{\delta \lambda(l, l')}{\delta \alpha(l)} dl'. \tag{7}$$

We argue below that the function  $\lambda(l, l')$  is a weak function of  $\alpha(l)$  such that the final term may be neglected. For an isotropic-nematic coexistence state to exist at equilibrium, two additional criteria must be satisfied. The two phases must have equal chemical potentials  $[\mu(l)/k_BT = \delta f/\delta c(l)]$  as a function of l, yielding the condition

$$\ln c^{(I)}(l) + 2lc_1^{(I)} = \ln c^{(N)}(l) + \ln \left[\alpha(l)\right] - 1 + \mu_{ex}^{(N)}(l), \tag{8}$$

and the excess chemical potential for the nematic phase  $\mu_{ex}^{(N)}(l)$  is defined as

$$\mu_{ex}^{(N)}(l) = l \int l'c(l')\lambda(l,l')dl' + 2^{3/2}l \int \frac{c^{(N)}(l')l'}{c_0^{(N)}} \sqrt{\tilde{\alpha}(l)^{-1} + \tilde{\alpha}(l')^{-1}}dl', \tag{9}$$

where  $\tilde{\alpha} = (\pi/4)(c_0^{(N)})^{-2}$ . This criteria must be fulfilled for all l. The two phases must also have the same osmotic pressure  $[\Pi = \delta f/\delta V]$  which yields the additional equation

$$c_0^{(I)} + \left(c_1^{(I)}\right)^2 = c_0^{(N)} + \int lc^{(N)}(l)l'c^{(N)}(l')[\rho(l,l') + \lambda(l,l')]dldl'. \tag{10}$$

Finally, conservation of mass must hold such that the two daughter phases in coexistence must add together to the parent population, i.e.,

$$c^{(0)}(l) = (1 - \gamma)c^{(I)}(l) + \gamma c^{(N)}(l), \tag{11}$$

where  $\gamma$  is the volumetric fraction of the system that is nematic. Given a starting population  $c^{(0)}(l)$  and attractive potential U(D), Eqs. (7, 8, 10, 11) comprise three functional equations and one scalar equation that may be solved for  $c^{(I)}(l)$ ,  $c^{(N)}(l)$ ,  $\alpha(l)$ , and  $\gamma$ . (Alternatively, the normalized parent population  $c^{(0)}(l)/c_0^{(0)}$  and  $\gamma$  may be specified with the quantity  $c_0^{(0)}$  as an unknown.) Note that the constant reference length  $L_0$  is defined relative to the parent population.

# 2.3 Attractive and Repulsive Interactions

The novel contribution to the free energy expression is expressed in the quantity  $\lambda(l)$ . We propose a particular phenomenological model inspired by the unusual "SWNT spaghetti" liquid crystalline phase illustrated in Figure 1; the SWNTs in these strands are aligned along the strand with small distances between SWNT sidewalls. The SWNTs are no longer in due to the short-range electrostatic repulsion, but the attractive forces keep them within a few diameters of each another, such that each SWNT interacts with an effective "cage" of other SWNTs within the liquid crystalline phase.

Our proposed model is as follows: A rod in an aligned state is subject to an attractive interaction with surrounding rods u(D), which represents the energy per unit length of the rod as a function of the distance D between the centers of the aligned rods. This quantity scales linearly with l and is made dimensionless as  $U(D) \equiv u(D)L_{mean}/k_BT$ , where  $L_{mean}$  is the average length of the parent population. The square-well potential U(D) is depicted in Figure 1 and is characterized by the four parameters  $U_{max}$ ,  $U_{min}$ ,  $D_1$ , and  $D_2$ . The discontinuities in the derivatives of the square-well potential are made continuous by using an arctan function to approximate the transitions of U(D) across  $D_1$  and  $D_2$ .

As a first approximation, this attractive interaction is applied only to the dense nematic phase. These interactions are expected to affect only minimally the free energy of the isotropic phase because the rods are less concentrated and unaligned. The attractive interaction varies weakly with alignment in nematic phases. On average, the nematic phase will behave much like a columnar phase where the average inter-rod distance D can be calculated from  $\phi^{(N)}$ , the rod volume fraction in the nematic phase, as

$$D = \frac{d}{2} \left( \frac{\phi^{(N)} \sqrt{3}}{2\pi} \right)^{-1/2}.$$
 (12)

As the "test" rod feels the attractive potential, the rod's nearest neighbors in the densely packed nematic phase will "shield" the rod from others that are farther out such that the attractive interaction is minimal beyond those nearest neighbors. (Also, those nearest neighbors will be the first to enter the repulsive region.) Consequently, the quantity  $lc(l) \int l'c(l')\lambda(l,l')dl'$  is rewritten as  $lc(l)\Lambda(l)$  where  $\Lambda(l) = 6(L_0/d)U(D)$ . (A similar argument is used by Wensink and Vroege in the case of average excluded volume in the nematic phase.) The square-well potential can be parameterized by the dimensionless quantities

 $U_{\text{max}}$ ,  $U_{\text{min}}$ ,  $D_1/d$ , and  $D_2/d$ , which may vary with solvent quality. In addition, the repulsive region  $(D < D_1)$  increases the effective excluded volume by a factor of (D + 1)/2.

#### 2.4 Shadow and Cloud Phases

The phase behavior of polydisperse rod populations is complicated by the fact that the parent population  $c^{(0)}(l)$  influences the properties of the daughter populations  $c^{(I)}(l)$  and  $c^{(N)}(l)$ . This stands in contrast to the monodisperse case where the coexistence values of  $c_0^{(I)}$  and  $c_0^{(N)}$  are independent of the parent concentration  $c_0^{(0)}$ .

Two useful but oft-misunderstood concepts for delineating the phase behavior of polydisperse rod populations are the cloud phase and shadow phase. For example, at small concentrations, a parent population of polydisperse rods in an athermal solvent will remain isotropic with no phase separation. As the parent concentration  $c_0^{(0)}$  is increased, a point is reached where an infinitesimal volume of nematic phase, termed a "shadow phase," forms while the vast majority of the parent population remains in the "cloud" isotropic phase. Thus, the shadow nematic phase coexists with the cloud isotropic phase, and the corresponding value of  $c_0^{(0)}$  represents the lowest value of  $c_0^{(0)}$  at which coexistence is possible. The converse is true on the high-concentration side of the phase diagram; the shadow isotropic phase coexists with the cloud nematic phase, and the corresponding value of  $c_0^{(0)}$ represents the highest value of  $c_0^{(0)}$  at which coexistence is possible. On the isotropic cloud curve, the quantity  $\gamma$  (the fraction of the system that is nematic) will approach zero, while on the nematic cloud curve,  $\gamma$  will approach one.

The isotropic and nematic cloud phases are the ultimate boundaries of the biphasic region

in a system of polydisperse rods. Parent populations within the biphasic region will phase separate into coexisting isotropic and nematic phases, and the values of  $c_0^{(I)}$  and  $c_0^{(N)}$  will vary with  $c_0^{(0)}$ . These concepts are illustrated in Fig. 2, which depicts the various types of phase separation that occur at the two cloud points in contrast with the  $c_0^{(0)}$ -independent phase boundaries observed in monodisperse systems. Note that the daughter phases appear to remain in the biphasic regime which suggests that they are not an equilibrium solution; this paradox is resolved by the fact that the daughters have a different length distribution than the parent phase, such that the daughter phases lie outside the cloud curves for their specific distribution.

#### 2.5 Parent Distribution and Solution Method

For the SWNT samples of interest, the parent rod population is well-described by a simple Schultz distribution

$$c^{(0)}(l)/c_0^{(0)} = Nl^z \exp[-(z+1)l], \tag{13}$$

with normalization factor N and is truncated at some minimum and maximum l. The polydispersity of any population is described by the parameter  $\sigma$ , defined as

$$\sigma^2 = c_2^{(0)} / \left(c_1^{(0)}\right)^2 - 1,\tag{14}$$

which is related to the parameter z in the Schultz distribution as  $\sigma^2 = (1+z)^{-1}$ .

In a typical purified batch of HiPco SWNTs (HPR batch 152.2), we find that the parent distribution of SWNTs is well-approximated through the Schultz distribution as follows: d = 1nm,  $L_{mean} = 348nm$ ,  $L_{min} = 17nm$  (the SWNT purification process eliminates SWNTs below a particular cutoff),  $L_{max} = 8\mu m$ , and  $\sigma = 0.6$  [37]. We use this as an example parent

population.

In general, we explore numerically the phase behavior of a SWNT-dispersion as a function of the attractive potential well depth  $U_{\min}$ , concentration  $\phi_0$ , and of the polydispersity  $\sigma$ . For all studies, we set  $U_{\max} \gg |U_{\min}|$  since variations in  $U_{\max}$  do not substantially change the phase behavior as long as  $U_{\max} > 1$ , and we set  $D_2/d \gg 1$  because nematic phases where  $D > D_2$  do not differ from the athermal case.

The l-space is discretized into Q points in a fashion similar to that described by Wensink and Vroege, and Eqs. (7, 8, 10, 11) are discretized into 3Q + 1 nonlinear equations and solved simultaneously using Newton's method. Solutions are traced in  $c_0^{(0)}$ -space (or  $\gamma$ -space),  $\sigma$ -space and  $U_{\min}$ -space using arclength continuation in the parameter of interest [19]. The following results and discussion are specific to the Schultz distribution but should be representative of the behavior of other parent populations.

# 3 Results & Discussion

#### 3.1 Cloud curves

For the example population of rods described above with  $\sigma = 0.6$ , the isotropic and nematic cloud curves are computed as a function of  $U_{\min}$  for the case where  $D_1/d = 1$  (Fig. 3).  $U_{\min} = 0$  corresponds to polydisperse athermal rods; the isotropic cloud point is  $\phi^{(I)} = 0.0049$ , and the nematic cloud point is  $\phi^{(N)} = 0.261$ .

As attractive interactions grow, the nematic phase becomes more thermodynamically favorable and more concentrated. Because  $D_1/d = 1$ , the aligned rods can pack tightly

together in the liquid crystalline phase, so the nematic cloud curve moves rapidly to  $\phi^{(N)} = 1$  as  $U_{\min}$  decreases. Setting  $D_1/d > 1$  essentially sets a minimum for inter-rod spacing and a maximum  $\phi^{(N)}$ . Such a case is shown as a dotted line in Fig. 3 for  $D_1/d = 1.76$ , where the increase in  $\phi^{(N)}$  is arrested by short-range repulsion.

The nematic cloud curve in Fig. 3 for  $D_1/d = 1$  is somewhat similar to the classic Flory theory [11] and the Khokhlov extension of the Onsager theory [9] because the biphasic region primarily broadens by increasing the concentration of the nematic cloud curve  $\phi^{(N)}$  toward 1 as the solvent quality decreases. In all these previous studies, the nematic concentration rapidly increases to a solid-like state because short-range repulsion is not included in the model.

Most interestingly, the isotropic cloud curve convergences to zero at a critical value of  $U_{\min}^* \cong -0.581$ . Therefore in systems where attractive interactions are stronger than this critical value, the dilute, isotropic phase must always coexist with some liquid-crystalline phase. Even at infinitesimal concentrations, the system is still in the biphasic regime; thus, some rods will form an aligned phase at equilibrium due to the strong attraction. This holds great import for experimental studies of rod dispersions, as discussed below.

Figures 4 and 5 show the influence of polydispersity  $\sigma$  on the isotropic and nematic cloud curves for  $D_1/d = 1$ . The monodisperse ( $\sigma \to 0$ ) limit is computed by Richardson extrapolation [38].

As polydispersity decreases, the isotropic cloud curves move down to lower well depths and to the right to higher rod concentration; this is to be expected since the effects of length fractionation decrease as polydispersity decreases. This also means that  $U_{\min}^*$  decreases as a function of  $\sigma$ ; this holds practical import for experimental scenarios where an isotropic

solution is desired. If a particular solvent/rod combination corresponds to a value of  $U_{\min}$  that is less than  $U_{\min}^*$ , then even dilute solutions will be in the biphasic regime. If the polydispersity of the solution can be decreased and/or the average length increased, then the value of  $U_{\min}^*$  will also decrease; thus, polydispersity can be used as a control to ensure that  $U_{\min} > U_{\min}^*$ .

As polydispersity decreases, the nematic cloud curve moves down to lower well depths and to the left to lower rod concentration. For low  $\sigma$ , the nematic cloud curve is a much weaker function of acid strength than the isotropic cloud curve. Thus, for broad distributions (e.g.,  $\sigma = 0.6$ ), the nematic cloud curve varies more rapidly than the isotropic cloud curve while for narrow distributions (e.g.,  $\sigma = 0.3$ ) the opposite is true.

# 3.2 Comparison with experiment

In previous papers, we used a series of experiments to establish a phase diagram for SWNT/acid mixtures [22, 17] which is displayed in Figure 6. Various SWNT/acid mixtures at a given SWNT concentration (denoted by diamonds in Figure 6) are centrifuged into isotropic and nematic phases, and the concentration  $\phi^{(I)}$  of the isotropic phase is measured and marked as black circles.  $\phi^{(I)}$  grows with increasing fractional charge (better solvent quality). The nematic cloud curve (black squares) is also measured by using light microscopy, dynamic rheology, steady shear rheology, and differential scanning calorimetry. In contrast with the predictions of Flory-like theories, the dilute isotropic phase in poor solvents coexists with a concentrated liquid-crystalline phase ( $\phi^{(N)} \approx 0.1$ ) rather than with a solid phase (i.e.,  $\phi^{(N)} > 0.9$ ).

<sup>&</sup>lt;sup>1</sup>Concentration is measured using UV-vis-NIR absorbance.[22]

In order to compare the theoretical results with experimental results for SWNTs in superacids, a relationship between  $U_{\min}$  and acid strength must be established. Superacid strength is typically measured in terms of base-specific Hammett acidity [39]. In the case of SWNT/superacid systems, acid strength is related to the fractional charge per carbon caused by protonation of the nanotube sidewall [22]. (This quantity can be related to the wavenumber shift, dG, of the G-peak in the SWNT Raman spectra.) Attractive van der Waals forces should be roughly independent of acid strength. However, as the degree of protonation increases, the repulsion effect increases, and the attractive well becomes shallower. The strength of the repulsive force between two SWNTs should depend approximately linearly on the fractional charge per carbon. Thus, a linear relationship may be established between dG and the attractive well depth  $U_{\min}$  by comparing the theoretical and experimental results for the isotropic concentration after phase separation.<sup>2</sup>

Experimental measurements for the strongest acid used (chlorosulfonic acid) indicate that  $\phi^{(I)}$  is approximately equal to the theoretical predictions for athermal (Onsager) rods; thus, we match a Raman shift of  $dG = 25cm^{-1}$  to  $U_{\min} = 0$ . The theoretical predictions for  $\phi^{(I)}$  for  $U_{\min} = -0.957$  match the values of  $\phi^{(I)}$  from centrifugation experiments on SWNTs in 102% H<sub>2</sub>SO<sub>4</sub> (i.e., 100% H<sub>2</sub>SO<sub>4</sub> with excess 2 wt% dissolved SO<sub>3</sub>) which has a Raman shift of  $dG = 17cm^{-1}$ . These two data points set the linear relationship between  $U_{\min}$  and dG.

 $<sup>^{2}</sup>$ A number of factors will influence the relationship between acid strength and  $U_{\min}$ , and these factors may vary from one SWNT sample to another.  $U_{\min}$  is independent of SWNT length and polydispersity, but experiments indicate that the solubility of a HiPco SWNT sample in a given acid varies with diameter distribution, the frequency of defects in the SWNT sidewalls, and the chemical effects of the oxidation and purification process on the SWNT sidewalls.

Figure 6 combines computational and experimental results in a full phase diagram for SWNT/acid mixtures.<sup>3</sup> The model (red open circles) is remarkably successful at predicting the experimental values  $\phi^{(I)}$  (black circles) at low concentrations [17]. Therefore, the linear relationship between  $U_{\min}$  and dG is reasonably accurate and the simple square-well potential captures the essence of the physical interactions between SWNTs in acids.

Additional experiments were performed to test the model. The concentration  $\phi^{(I)}$  of the isotropic phase in 120%  $H_2SO_4$  was measured as a function of the starting concentration  $\phi^{(0)}$ . A comparison between theoretical and experimental data points is displayed in Figure 7. Again, the agreement between the two shows that the fundamental physics of internanotube interactions are captured by the theory.

An example of length fractionation as predicted by the theory is shown in Figure 8 with shorter rods selectively going into the isotropic phase and longer rods selectively going into the nematic phase.

Experimental measurements indicate a nematic cloud point of  $\phi^{(N)} \approx 0.1$  that is relatively constant with respect to acid strength; however, the theoretical results indicate a higher constant value of  $\phi^{(N)} = 0.152.^4$  Unlike the case of low-concentration phase separation, the theoretical and experimental values for the nematic cloud curve do not match. However, further analysis of the theoretical results reveals why the values differ. In Fig. 9, the theory predicts that  $\gamma \approx 0.99$  for a system where  $\phi^{(0)} = 0.1$ , i.e., 99% of the system (by

 $<sup>^{3}</sup>$ The computational results are for the example parent population described in section 2.5.

 $<sup>^4</sup>D_1/d$  is set to a constant value of 2.44, independent of acid strength. This choice is influenced by two considerations. First, the maximum packing fraction should not vary with acid strength. Second, the experimentally measured nematic cloud curve is independent of acid strength. The choice of  $D_1/d = 2.44$  sets the maximum packing fraction to be the same as the athermal nematic cloud curve.

volume) is nematic. The remaining 1% is isotropic and comprised of relatively short rods, as shown in Fig. 10. In an experiment, these short-rod-dominated isotropic regions would be found primarily in the defects between liquid-crystalline domains, and these small isotropic regions would be nearly undetectable by optical microscopy, rheology, or DSC. Thus, the experimental points are best taken as measurements of the transition to a system that is 99% liquid crystalline by volume, and we may take the theoretical prediction of the nematic cloud point as correct. The theory predicts that the starting concentration must be pushed all the way to  $\phi^{(0)} = 0.152$  to completely eliminate these isotropic regions. Such a high concentration may be experimentally impractical because the acid may not be able to fully protonate such a high SWNT concentration. (This has been confirmed for  $102-120\% \text{ H}_2\text{SO}_4$ .) However, simulation results also indicate that if all of the rods with an aspect ratio under 40 are removed, then the nematic cloud curve decreases to  $\phi^{(0)} \approx 0.1$ .

# 3.3 Applications

The computational results show that a liquid-crystalline phase will always be present for acids with  $dG < 20.15cm^{-1}$  ( $U_{\min} < U_{\min}^*$ , where  $U_{\min}^* = -0.581$ , equivalent to an acid mixture with a 9:16 volume ratio of ClSO<sub>3</sub>H to H<sub>2</sub>SO<sub>4</sub>), regardless of the starting SWNT concentration. This means that in order to get a dilute, isotropic suspension of individual SWNTs in superacid, the solution must first be centrifuged and phase separated in order to remove the isotropic phase from the nematic phase. A number of CNT characterization techniques (such as rheological characterization of CNT length [40]) require a dilute, isotropic suspension, and these counterintuitive computational results show that a simple

low-concentration dispersion of SWNTs in 120% H<sub>2</sub>SO<sub>4</sub> will not yield a dilute, isotropic solution. The isotropic cloud curve can be moved down to lower well depths and to the right to higher rod concentrations by eliminating the longest SWNTs in a given sample; this would be useful for applications requiring a dilute, isotropic solution and could be accomplished via a number of experimental techniques.

Also, one of the chief applications of SWNT / superacid dispersions is the formation of aligned articles such as fibers and films [30, 17]; our computational results have immediate applications for the processing of such articles. The fiber spinning process works as follows: High-concentration, liquid-crystalline SWNT / superacid dispersions are mixed, and extruded. The viscous dispersion becomes more aligned due to the tension on the fluid during extensional flow. Finally, the dispersion is coagulated in a non-solvent bath where the acid is removed, and the SWNT dispersion solidifies to form an aligned fiber. The best fibers are produced by dispersions that are highly aligned and fully liquid-crystalline, i.e., above the nematic cloud curve. Any isotropic regions in the dispersions form misaligned, weak regions in the final fiber; these defects decrease the electrical properties and are the primary points of fiber mechanical failure. (Note that defects that are predominantly composed of small nanotubes have already been observed for liquid-crystalline MWNT systems [41].)

With this application in mind, the theoretical framework outlined above can be used to locate the true nematic cloud curve in order to ensure that the dispersion is fully liquid crystalline. In this case, the cloud curve concentration may be too high for practical mixing and fiber spinning, so the theoretical framework can also be used to test the results of manipulating the starting SWNT length distribution in order to decrease the nematic cloud

concentration. In this case, the elimination of SWNTs under 40nm will decrease the nematic cloud concentration to  $\phi^{(0)} \approx 0.1$  such that SWNT/superacid dopes of  $\phi^{(0)} \approx 0.1$  will be fully liquid crystalline.<sup>5</sup>

Also, this theoretical framework has implications for high-concentration rheology of SWNT dispersions. The dependence of viscosity on concentration is a well-known experimental test for liquid-crystallinity; the viscosity increases, goes through a maximum, decreases due to the formation of a liquid-crystalline phase, and finally begins to increase again at high concentrations [24]. This dependence on concentration is blurred and weak-ened as the biphasic chimney is broadened because the formation of aligned phase occurs over a much wider concentration range. SWNT/superacid dispersions with weaker acids or poly-disperse length distributions will show a weak dependence of viscosity on concentration and may not show the maximum/minimum signature of liquid-crystallinity. Decreasing poly-dispersity or strengthening the acid solvent will sharpen and amplify the difference between the maximum and minimum in viscosity.

The utility of the theoretical treatment outlined in this study is evident from the unexpected nature of the results. Optical microscopy experiments and DSC could not detect the isotropic regions in the SWNT/superacid dispersions used for fiber spinning at  $\phi^{(0)} \approx 0.1$ , but the theory predicts that these regions are indeed present; such regions have adverse effects on as-spun fibers. Also, it is entirely intuitive to reason that a dilute solution of SWNTs in  $\overline{\phantom{a}}$  This may be accomplished by a numerical of experimental techniques. These include washing the initial SWNT sample with a weaker acid (such as 98% H<sub>2</sub>SO<sub>4</sub>) to eliminate the shortest SWNTs. Also, fractionating a sample in the biphasic regime in a weaker superacid (such as 102% H<sub>2</sub>SO<sub>4</sub>) and removing the isotropic phase can be used to eliminate the shortest SWNTs.

120% H<sub>2</sub>SO<sub>4</sub> would be dispersed as isotropic individuals, but the theory predicts that even these low concentrations are within the biphasic region because of attractive interactions.

We expect that this analysis will pave the way for the modeling of other anisotropic materials such as multi-walled carbon nanotubes (MWNTs) or inorganic nanorods. The phase behavior of CdSe nanorods [42] has been assessed through purely qualitative means, and an effective theoretical framework for understanding these materials is needed. The phase transitions for solutions of polydisperse functionalized MWNTs were qualitatively characterized by Song and Windle [43, 44]. A theoretical analysis of these systems may allow a more quantitative understanding of these dispersed nanomaterials.

#### 3.4 Conclusions

We have developed an extension to the Onsager theory for polydisperse rigid rods developed by Wensink and Vroege in order to capture the balance of long-range attractive and repulsive forces observed for anisotropic nanomaterials in solution. Our work is particularly motivated by the recent quantitative experimental data for SWNTs dispersed as individual rigid rods in superacids. Our results indicate excellent agreement between the theory and experimental data for predicting phase separation at low concentrations and for predicting the biphasic chimney's broadening on the isotropic side. The theoretical results also hold important and surprising implications for a variety of SWNT/superacid experiments and applications, including the understanding of SWNT/superacid rheology and the processing of fibers and films from liquid crystalline dopes.

#### Acknowledgments

We acknowledge the help of Virginia Davis, Pradeep Rai, Valentin Prieto, Howard Schmidt, Richard Booker, Hua Fan, Robert Hauge, Rick Smalley, and Wade Adams. Funding was provided by the Office of Naval Research under Grant N00014-01-1-0789, AFOSR grant FA9550-06-1-0207, AFRL agreements FA8650-07-2-5061 and 07-S568-0042-01-C1, NSF CAREER, and the Evans-Attwell Welch Postdoctoral Fellowship. This material is based on research sponsored by Air Force Research Laboratory under agreement number FA8650-07-2-5061.

# References

- [1] Z. Dogic, K. R. Purdy, E. Grelet, M. Adams, and S. Fraden. Isotropic-nematic phase transition in suspensions of filamentous virus and the neutral polymer dextran. *Phys. Rev. E*, 69:051702, 2004.
- [2] L. Onsager. The effects of shape on the interaction of colloidal particles. Ann. N.Y. Acad. Sci., 51:627, 1949.
- [3] R. F. Kayser and H. J. Raveche. Bifurcation in onsager's model of the isotropic-nematic transition. *Phys. Rev. A.*, 17:2067–2072, 1978.
- [4] H. N. W. Lekkerkerker, P. Coulon, R. Van Der Haegen, and R. Deblieck. On the isotropic-liquid crystal phase separation in a solution of rodlike particles of different lengths. J. Chem. Phys., 80:3427–3433, 1984.
- [5] Z. Y. Chen and J. Noolandi. Numerical solution of the onsager problem for an isotropic-nematic interface. *Phys. Rev. A*, 45:2389–2392, 1980.

- [6] D. L. Koch and O. G. Harlen. Interfacial tension at the boundary between nematic and isotropic phases of a hard rod solution. *Macromol.*, 32:219–226, 1999.
- [7] K. Shundyak and R. van Roij. Isotropic-nematic interfaces of hard-rod fluids. J. Phys.: Condens. Matter, 13:4789–4800, 2001.
- [8] M. J. Green, R. C. Armstrong, and R. A. Brown. Computation of the nonhomogeneous equilibrium states of a rigid-rod solution. *J. Chem. Phys.*, 125:214906, 2006.
- [9] A. R. Khokhlov. Theories based on the onsager approach. In A. Ciferri, editor, Liquid Crystallinity in Polymers, New York, 1991. VCH.
- [10] A. R. Khokhlov and A. N. Semenov. Statistical physics of liquid-crystalline polymers. J. Stat. Phys., 38:161–182, 1985.
- [11] P. J. Flory. Phase equilibria in solutions of rod-like particles. Proc. Roy. Soc. London A, 234:73–89, 1956.
- [12] P. J. Flory. Statistical thermodynamics of semi-flexible chain molecules. Proc. Roy. Soc. London A, 234:60-73, 1956.
- [13] P. J. Flory. Statistical thermodynamics of mixtures of rodlike particles. 5. mixtures with random coils. *Macromol.*, 11:1138–1141, 1978.
- [14] P. J. Flory. Statistical thermodynamics of mixtures of rodlike particles. 6. rods connected by flexible joints. *Macromol.*, 11:1141–1144, 1978.
- [15] M. Ballauff. Phase equilibria in rodlike systems with flexible side chains. *Macromol.*, 19:131–160, 1995.

- [16] P. J. Flory and A. Abe. Statistical thermodynamics of mixtures of rodlike particles. 1. theory for polydisperse systems. *Macromol.*, 11:1119–1122, 1978.
- [17] V. A. Davis, A. N. G. Parra Vasquez, M. J. Green, P. K. Rai, N. Behabtu, V. Prieto, R. D. Booker, J. Schmidt, E. Kesselman, W. Zhou, H. Fan, W. W. Adams, R. H. Hauge, J. E. Fischer, Y. Cohen, Y. Talmon, R. E. Smalley, and M. Pasquali. Controlling swnt/superacid phase behavior for the bottom-up assembly of nanomaterials. in preparation, 2009.
- [18] M. Surve, V. Pryamitsin, and V. Ganesan. Dispersion and percolation transitions of nanorods in polymer solutions. *Macromol.*, 40:344–354, 2007.
- [19] P. G. Bolhuis, A. Stoobants, D. Frenkel, and H. N. W. Lekkerkerker. Numerical study of the phase behavior of rodlike colloids with attractive interactions. *J. Chem. Phys.*, 107(5):1551–1564, 1997.
- [20] A. Speranza and P. Sollich. Isotropic-nematic phase equilibria in the onsager theory of hard rods with length polydispersity. *Phys. Rev. E*, 67:061702, 2002.
- [21] H. H. Wensink and G. J. Vroege. Isotropic-nematic phase behavior of length-polydisperse hard rods. *J. Chem. Phys.*, 119:6868–6882, 2003.
- [22] P. K. Rai, R. A. Pinnick, A. N. G. Parra-Vasquez, V. A. Davis, H. K. Schmidt, R. H. Hauge, R. E. Smalley, and M. Pasquali. Isotropic-nematic phase transition of single-walled carbon nanotubes in strong acids. J. Am. Chem. Soc., 128:591–595, 2006.
- [23] S. Ramesh, L. M. Ericson, V. A. Davis, R. K. Saini, C. Kittrell, M. Pasquali, W. E. Billups, W. W. Adams, R. H. Hauge, and R. E. Smalley. Dissolution of pristine sin-

- gle walled carbon nanotubes in superacids by direct protonation. *J. Phys. Chem. B*, 108:8794–8798, 2004.
- [24] V. A. Davis, L. M. Ericson, A. N. G. Parra-Vasquez, H. Fan, Y. Wang, V. Prieto, J. A. Longoria, S. Ramesh, R. K. Saini, C. Kittrell, W. E. Billups, W. W. Adams, R. H. Hauge, R. E. Smalley, and M. Pasquali. Phase behavior and rheology of swnts in superacids. *Macromol.*, 37:154–160, 2004.
- [25] S. Iijima and T. Ichihashi. Single-shell carbon nanotubes of 1-nm diameter. *Nature*, 363:603–605, 1993.
- [26] R. H. Baughman. Putting a new spin on carbon nanotubes. Science, 290:1310–1311, 2000.
- [27] S. Badaire, C. Zakri, M. Maugey, A. Derre, J. N. Barisci, G. G. Wallace, and P. Poulin. Liquid crystals of dna-stabilized carbon nanotubes. Adv. Mater., 17:1673–1676, 2005.
- [28] S. E. Moulton, M. Maugey, P. Poulin, and G. G. Wallace. Liquid crystal behavior of single-walled carbon nanotubes dispersed in biological hyaluronic acid solutions. J. Am. Chem. Soc., 129:9452–9457, 2007.
- [29] M. F. Islam, A. M. Alsayed, Z. Dogic, J. Zhang, T. C. Lubensky, and A. G. Yodh. Nematic nanotube gels. Phys. Rev. Lett., 92:088303, 2004.
- [30] L. M. Ericson, H. Fan, H. Peng, V. A. Davis, W. Zhou, J. Sulpizio, Y. Wang, R. Booker, J. Vavro, C. Guthy, A. N. G. Parra-Vasquez, M. J. Kim, S. Ramesh, R. K. Saini, C. Kittrell, G. Lavin, H. Schmidt, W. W. Adams, W. E. Billups, M. Pasquali, W.-F.

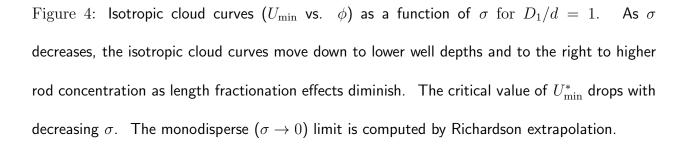
- Hwang, R. H. Hauge, J. E. Fischer, and R. E. Smalley. Macroscopic, neat, single-walled carbon nanotube fibers. *Science*, 305:1447–1450, 2004.
- [31] N. Behabtu, M.J. Green, and M. Pasquali. Carbon nanotube-based fibers. *Nano Today*, 3:24–34, 2008.
- [32] E. J. W. Verwey and J. T. G. Overbeek. Theory of the Stability of Lyophobic Colloids. Elsevier, Amsterdam, 1948.
- [33] J. N. Israelachvili. Intermolecular and Surface Forces. Academic Press, London, 1992.
- [34] D. Chapot, L. Bocquet, and E. Trizac. Interaction between charged anisotropic macro-molecules: Application to rod-like polyelectrolytes. J. Chem. Phys., 120:3969–3982, 2004.
- [35] O. Pelletier, P. Davidson, C. Bourgaux, and J. Livage. The effect of attractive interactions on the nematic order of v2o5 gels. *Europhys. Lett.*, 48:53–39, 1999.
- [36] H. Maeda and Y. Maeda. Measurement of density distributions for colloidal b-feooh rods in suspensions exhibiting phase separation: The role of long-range forces in smectic ordering. J. Chem. Phys., 121:12655, 2004.
- [37] V. A. Davis. Phase Behavior and Rheology of Single-Walled Carbon Nanotubes (SWNTs) in Superacids with Application to Fiber Spinning. PhD thesis, Rice University, 2006.
- [38] H. Jeffreys and B. S. Jeffreys. Methods of Mathematical Physics, 3rd ed. Cambridge University Press, 1988.

- [39] Y. Marcus, E. Pross, and N. Soffer. Ionic dissociation of hydrobromic acid. 3. hammett acidity function, h0, of hydrobromic acid and its ionic dissociation. *J. Phys. Chem.*, 84:1725–1729, 1980.
- [40] A. N. G. Parra-Vasquez, I. Stepanek, V. A. Davis, V. C. Moore, E. H. Haroz, J. Shaver, R. H. Hauge, R. E. Smalley, and M. Pasquali. Simple length determination of singlewalled carbon nanotubes by viscosity measurements in dilute suspensions. *Macromol.*, 40:4043–4047, 2007.
- [41] S. J. Zhang, I. A. Kinloch, and A. H. Windle. Mesogenicity drives fractionation in lyotropic aqueous suspensions of multiwall carbon nanotubes. *Nano Lett.*, 6:568–572, 2006.
- [42] L. Li, M. Marjanska, G. H. J. Park, A. Pines, and A. P. Alivisatos. Isotropic-liquid crystalline phase diagram of a cdse nanorod solution. J. Chem. Phys., 120:1149–1152, 2004.
- [43] W. Song and A. H. Windle. Isotropic-nematic phase transition of dispersions of multiwall carbon nanotubes. *Macromol.*, 38:6181–6188, 2005.
- [44] W. Song, I. A. Kinloch, and A. H. Windle. Nematic liquid crystallinity of multiwall carbon nanotubes. *Science*, 302:1363, 2003.

Figure 1: (I) The combination of short range electrostatic repulsive forces (shown in blue) and van der Waals attraction will result in an attractive well (shown in red) potential between the two particles. However, the exact form of these functions is unknown for complex solvent and solutes such as superacids and SWNTs. (II) A simple, phenomenological square well potential U(D) is used to capture this balance of repulsive forces and attractive forces between SWNTs in various acids. As the acid quality decreases, the well becomes deeper. (III) D is the distance between neighboring SWNTs in the liquid-crystalline phase. This simplified potential is inspired by the unusual liquid-crystalline order seen in "spaghetti" in SWNT/superacid systems [24]. (IV) A schematic of "spaghetti" geometry depicts the threadlike, aligned nature of these unusual liquid-crystalline domains.

Figure 2: Simple illustration of the difference between monodisperse and polydisperse rod systems. In the monodisperse case, the concentrations of the isotropic and nematic phases are independent of the initial concentration  $\phi^{(0)}$  within the biphasic region. In the polydisperse case, the phase concentrations are dependent on  $\phi^{(0)}$ , and the ultimate boundaries of the biphasic region occur at the isotropic cloud point (where  $\phi^{(0)} = \phi^{(I)}$ ) and the nematic cloud point (where  $\phi^{(0)} = \phi^{(N)}$ ).

Figure 3: The isotropic and nematic cloud points are depicted as a function of the well depth  $U_{\min}$  for  $\sigma=0.6,\,L_{mean}=348d.$  When  $D_1/d=1$ , the nematic cloud point rapidly increases to  $\phi^{(N)}=1$  as  $U_{\min}$  decreases. For the case  $D_1/d=2.08$ ,  $\phi^{(N)}$  remains constant at 0.191. The Onsager predictions for monodisperse rods are depicted as triangles ( $\triangle$ ).



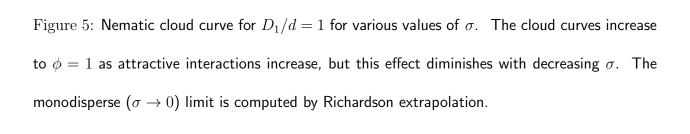


Figure 6: SWNT/superacid phase behavior as a function of SWNT volume fraction and acid strength (measured by dG). Black symbols denote experimental results [17]. Red symbols refer to theoretical predictions, and red open circles ( $\circ$ ) designate the theoretical predictions for  $\phi^{(I)}$  compared with experimental measurements of  $\phi^{(I)}$ , denoted by black circles ( $\bullet$ ). Black/red diamonds ( $\diamond$ ) indicate the initial system concentration  $\phi^{(0)}$  for both experiments and simulations of isotropic (I) - liquid crystalline (LC) phase separation. The open red triangles ( $\triangle$ ) is the Onsager predictions for  $\phi^{(I)}$  for a system of monodisperse hard-rods. A red line (-) represents the theoretical predictions for the isotropic cloud curve. Simulations are for  $\sigma=0.6$ ,  $L_{mean}=348d$ ,  $D_1/d=2.44$ .

Figure 7: SWNT/120  $H_2SO_4$  mixtures of varying  $\phi^{(0)}$  were prepared and phase separated; the isotropic concentration  $\phi^{(0)}$  was measured by UV-vis-NIR. These experimental measurements showed a close match with theoretical predictions ( $\sigma=0.6$ ,  $L_{mean}=348d$ ) for phase separation as a function of  $\phi^{(0)}$ .

Figure 8: Length fractionation is illustrated for  $(U_{\min}=0, \ \phi^{(0)}=0.0158, \ \sigma=0.6, \ L_{mean}=348nm, \ D_1/d=1)$ . The theory predicts phase separation into a nematic phase  $(\phi^{(N)}=0.0207, \ \sigma^{(N)}=0.4842, \ \langle L^{(N)}\rangle=434.6)$  and an isotropic phase  $(\phi^{(I)}=0.0086, \ \sigma^{(I)}=0.4744, \ \langle L^{(I)}\rangle=203.0)$ . Each of the distributions are normalized to 1.

Figure 9: Volumetric fraction of system that is nematic (denoted as  $\gamma$ ) as a function of  $\phi^{(0)}$  for for  $U_{\min}=0$ ,  $\sigma=0.6$ ,  $L_{mean}=348d$ ,  $D_1/d=2.44$ . The system reaches  $\gamma=0.99$  at  $\phi^{(0)}\approx0.1$  (noted as  $\blacktriangle$ ), but the concentration must increase all the way to  $\phi^{(0)}=0.152$  in order to reach  $\gamma=1$  (the nematic cloud point, noted as  $\spadesuit$ ). Experimental data indicates a cloud point of  $\phi^{(0)}\approx0.1$  but cannot detect the small isotropic regions filled with short rods that persist up to  $\phi^{(0)}=0.152$ .

Figure 10: Average length of rods in the isotropic phase (denoted as  $\langle L_I \rangle$ ) as a function of  $\phi^{(0)}$  for  $U_{\min}=0$ ,  $\sigma=0.6$ ,  $L_{mean}=348d$ ,  $D_1/d=2.44$ . Near the isotropic cloud point,  $\langle L_I \rangle$  approaches that of the parent population, but  $\langle L_I \rangle$  decreases dramatically as  $\phi^{(0)}$  approaches the nematic cloud point. Thus, near the nematic cloud point, the rods in the isotropic phase tend to be the shortest rods in the parent distribution.

